$N = 32$ shell closure below calcium: Low-lying structure of ^{50}Ar

M. L. Cortés,[1,2,*] W. Rodriguez,[3,1,4] P. Doornenbal,[1] A. Obertelli,[5,6] J. D. Holt,[7,8] J. Menéndez,[9,10] K. Ogata,[11,12]
A. Schwenk,[6,13,14] N. Shimizu,[9] J. Simonis,[15] Y. Utsuno,[16,9] K. Yoshida,[16] L. Achouri,[17] H. Baba,[1] F. Browne,[1] D. Calvet,[5]
F. Château,[5] S. Chen,[18,1] N. Chiga,[1] A. Corsi,[5] A. Delbart,[5] J.-M. Gheller,[5] A. Giganon,[5] A. Gillibert,[5] C. Hilaire,[5] T. Isobe,[1]
T. Kobayashi,[19] Y. Kubota,[1,9] V. Lapoux,[5] H. N. Liu,[5,6,20] T. Motobayashi,[1] I. Murray,[21,1] H. Otsu,[1] V. Panin,[1] N. Paul,[5]
H. Sakurai,[1,22] M. Sasano,[1] D. Steppenbeck,[1] L. Stuhl,[9,23] Y. L. Sun,[5,6] Y. Togano,[24] T. Uesaka,[1] K. Wimmer,[22] K. Yoneda,[1]
O. Aktas,[20] T. Aumann,[6,25] L. X. Chung,[26] F. Flavigny,[21] S. Franchoo,[21] I. Gašparić,[27,1] R.-B. Gerst,[28] J. Gibelin,[17]
K. I. Hahn,[29] D. Kim,[29] T. Koiwai,[22] Y. Kondo,[30] P. Koseoglou,[6,25] J. Lee,[31] C. Lehr,[6] B. D. Linh,[26] T. Lokotko,[31]
M. MacCormick,[21] K. Moschner,[28] T. Nakamura,[30] S. Y. Park,[29] D. Rossi,[6] E. Sahin,[32] P.-A. Söderström,[6] D. Sohler,[23]
S. Takeuchi,[30] H. Toernqvist,[6,25] V. Vaquero,[33] V. Wagner,[6] S. Wang,[34] V. Werner,[6] X. Xu,[31] H. Yamada,[30] D. Yan,[34] Z. Yang,[1]
M. Yasuda,[30] and L. Zanetti[6]

[1]*RIKEN Nishina Center, 2-1 Hirosawa, Wako, Saitama 351-0198, Japan*
[2]*Istituto Nazionale di Fisica Nucleare, Laboratori Nazionali di Legnaro, I-35020 Legnaro, Italy*
[3]*Departamento de Física, Facultad de Ciencias, Universidad Nacional de Colombia, Sede Bogota, Bogotá, Colombia*
[4]*Departamento de Física, Facultad de Ciencias, Pontificia Universidad Javeriana, Bogotá, Colombia*
[5]*IRFU, CEA, Université Paris-Saclay, F-91191 Gif-sur-Yvette, France*
[6]*Institut für Kernphysik, Technische Universität Darmstadt, 64289 Darmstadt, Germany*
[7]*TRIUMF, 4004 Wesbrook Mall, Vancouver, British Columbia V6T 2A3, Canada*
[8]*Department of Physics, McGill University, 3600 Rue University, Montréal, Quebec H3A 2T8, Canada*
[9]*Center for Nuclear Study, The University of Tokyo, RIKEN Campus, Wako, Saitama 351-0198, Japan*
[10]*Departament de Física Quàntica i Astrofísica, Universitat de Barcelona, 08028 Barcelona, Spain*
[11]*Research Center for Nuclear Physics (RCNP), Osaka University, Ibaraki 567-0047, Japan*
[12]*Department of Physics, Osaka City University, Osaka 558-8585, Japan*
[13]*ExtreMe Matter Institute EMMI, GSI Helmholtzzentrum für Schwerionenforschung GmbH, 64291 Darmstadt, Germany*
[14]*Max-Planck-Institut für Kernphysik, Saupfercheckweg 1, 69117 Heidelberg, Germany*
[15]*Institut für Kernphysik and PRISMA Cluster of Excellence, Johannes Gutenberg-Universiätat, Mainz 55099, Germany*
[16]*Advanced Science Research Center, Japan Atomic Energy Agency, Tokai, Ibaraki 319-1195, Japan*
[17]*LPC Caen, ENSICAEN, Université de Caen, CNRS/IN2P3, F-14050 Caen, France*
[18]*State Key Laboratory of Nuclear Physics and Technology, Peking University, Beijing 100871, China*
[19]*Department of Physics, Tohoku University, Sendai 980-8578, Japan*
[20]*Department of Physics, Royal Institute of Technology, SE-10691 Stockholm, Sweden*
[21]*IPN Orsay, CNRS and Université Paris-Saclay, F-91406 Orsay Cedex, France*
[22]*Department of Physics, University of Tokyo, 7-3-1 Hongo, Bunkyo, Tokyo 113-0033, Japan*
[23]*Institute for Nuclear Research (Atomki), P.O. Box 51, Debrecen H-4001, Hungary*
[24]*Department of Physics, Rikkyo University, 3-34-1 Nishi-Ikebukuro, Toshima, Tokyo 172-8501, Japan*
[25]*GSI Helmholtzzentrum für Schwerionenforschung GmbH, Planckstraße 1, 64291 Darmstadt, Germany*
[26]*Institute for Nuclear Science & Technology, VINATOM, P.O. Box 5T-160, Nghia Do, Hanoi, Vietnam*
[27]*Ruđer Bošković Institute, Bijenička cesta 54, 10000 Zagreb, Croatia*
[28]*Institut für Kernphysik, Universität zu Köln, D-50937 Cologne, Germany*
[29]*Department of Science Education and Department of Physics, Ewha Womans University, Seoul 03760, Korea*
[30]*Department of Physics, Tokyo Institute of Technology, 2-12-1 O-Okayama, Meguro, Tokyo 152-8551, Japan*
[31]*Department of Physics, The University of Hong Kong, Pokfulam, Hong Kong*
[32]*Department of Physics, University of Oslo, N-0316 Oslo, Norway*
[33]*Instituto de Estructura de la Materia, CSIC, E-28006 Madrid, Spain*
[34]*Institute of Modern Physics, Chinese Academy of Sciences, Lanzhou, China*

---

*liliana.cortes@lnl.infn.it

Low-lying excited states in the $N = 32$ isotope ^{50}Ar were investigated by in-beam γ-ray spectroscopy following proton- and neutron-knockout, multinucleon removal, and proton inelastic scattering at the RIKEN Radioactive Isotope Beam Factory. The energies of the two previously reported transitions have been confirmed, and five additional states are presented for the first time, including a candidate for a 3^- state. The level scheme built using $\gamma\gamma$ coincidences was compared to shell-model calculations in the sd-pf model space and to *ab initio* predictions based on chiral two- and three-nucleon interactions. Theoretical proton- and neutron-knockout cross sections suggest that two of the new transitions correspond to 2^+ states, while the previously proposed 4_1^+ state could also correspond to a 2^+ state.

I. INTRODUCTION

Our understanding of the atomic nucleus has as one of its cornerstones the concept of shell structure, in which the location of single-particle orbitals defines shell closures and associated magic numbers. Experimental evidence collected in the past decades, particularly since the advent of radioactive ion beams, has shown that shell structure undergoes significant changes for isotopes far from stability [1]. Examples of this shell evolution are the onset of $N = 16$ as a magic number for O isotopes [2–4] and the disappearance of the canonical magic number $N = 20$ around ^{32}Mg [5,6].

A particularly interesting case to study shell evolution is the region around the Ca isotopes between $N = 28$ and $N = 40$, where the development of shell closures for $N = 32$ and $N = 34$ has recently gained significant attention. In the Ca isotopes, the $N = 32$ subshell closure was first evidenced by its relatively high $E(2_1^+)$ energy [7], and confirmed by two-proton knockout cross section [8] and mass measurements [9]. In turn, the first suggestion of the $N = 34$ shell closure on ^{54}Ca was also provided by the $E(2_1^+)$ measurement [10] and confirmed by systematic mass measurements [11] and neutron-knockout reactions [12].

The persistence of these shell closures below and above $Z = 20$ has also been widely investigated. The preservation of the $N = 32$ shell closure above Ca has been determined in Ti and Cr via spectroscopy [13,14], reduced transition probabilities [15,16], and precision mass measurements [17]. On the other hand, the $N = 34$ shell closure has been suggested to disappear above Ca [18]. This is in contrast with the recently reported first spectroscopy measurement on ^{52}Ar, where the experimental value of $E(2_1^+)$ suggests the conservation of the $N = 34$ shell closure for $Z = 18$ [19].

The first spectroscopy of ^{50}Ar showed a relatively high $E(2_1^+)$ energy of 1178(18) keV [20]. In that study, apart from the $E(2_1^+)$, an $E(4_1^+)$ was tentatively assigned, although the limited statistics prevented a firmer conclusion [20]. No further spectroscopic information is available for this very exotic nucleus. The increase of the $E(2_1^+)$ with respect to neighboring isotopes has been interpreted as an indication of a sizable $N = 32$ gap along the Ar isotopic chain, therefore maintaining this subshell closure below ^{52}Ca [20].

From a theoretical point of view, the tensor-force-driven shell evolution has been used to explain the appearance of the $N = 32$ and $N = 34$ shell closures [21]. In this framework, the reduction of the attractive proton-neutron interaction between the $\pi f_{7/2}$ and the $\nu f_{5/2}$ single-particle orbitals results in a

separation between these levels and the formation of substantial neutron gaps. Calculations including this effect [22,23] successfully reproduce the $E(2_1^+)$ of Ar isotopes [19,20] and suggest the magnitude of the $N = 34$ subshell closure in ^{52}Ar to be around 3 MeV.

The significance of three-nucleon forces (3NFs) in the description of neutron-rich isotopes has also been studied [24,25], and the relevance of this contribution to obtain an accurate description of the spectroscopic properties of Ca isotopes has been highlighted [26]. In particular, *ab initio* calculations with the valence-space in-medium similarity renormalization group (VS-IMSRG) method [27–29] including 3NFs have provided a satisfactory description of the $E(2_1^+)$ along the Ar isotopic chain [19].

Our understanding of the nature of these subshell closures relies on the interpretation provided by the theoretical calculations. The validity of this picture can be further tested by studying its agreement with other nuclear properties, for example, the energies of low-lying states beyond the 2_1^+. To get a better insight into the structure at the $N = 32$ shell closure below Ca, the present work reports low-lying states in ^{50}Ar populated following direct and indirect reactions.

II. EXPERIMENT

The experiment was performed at the Radioactive Isotope Beam Factory, operated by the RIKEN Nishina Center and the Center for Nuclear Study of the University of Tokyo. A ^{70}Zn beam with an energy of 345 MeV/nucleon and an average intensity of 240 p nA was fragmented on a 3-mm-thick Be target to produce the secondary beam cocktail. Fragments of interest were selected by the BigRIPS separator [30] using the $B\rho$-ΔE-$B\rho$ technique. Event-by-event identification was obtained by an energy-loss measurement in an ionization chamber, position and angle measurements with parallel plate avalanche counters, at different focal planes, and the time of flight measured between two plastic scintillators [30]. The selected isotopes were focused in front of the SAMURAI dipole magnet [31], where the 151.3(13)-mm-long liquid hydrogen target of MINOS [32,33] was placed. Thanks to the use of a time projection chamber surrounding the target, it was possible to reconstruct the reaction vertex with a resolution of 2 mm (σ) [33]. Following the reactions in the target, ions were identified using the SAMURAI magnet and associated detectors. Positions and angles were measured at two multi-wire drift chambers placed in front and behind the magnet;

TABLE I. Inclusive cross sections (σ_{inc}) obtained for each of the reaction channels populating ^{50}Ar. The total number of events measured in each channel, the mean incident beam energy (E_{beam}), as well as the efficiency of MINOS ($\varepsilon_{\text{MINOS}}$) are listed.

Reaction	Events	E_{beam} (MeV/u)	$\varepsilon_{\text{MINOS}}$ (%)	σ_{inc} (mb)
^{52}Ca$(p, 3p)$ ^{50}Ar	132	266	99(12)	0.09(1)
^{53}Ca$(p, 3pn)$ ^{50}Ar	999	258	82(8)	0.33(3)
^{54}Ca$(p, 3p2n)$ ^{50}Ar	1393	251	88(8)	0.81(7)
^{55}Ca$(p, 3p3n)$ ^{50}Ar	790	247	85(3)	1.04(4)
^{51}K$(p, 2p)$ ^{50}Ar	28177	257	92(2)	3.9(1)
^{52}K$(p, 2pn)$ ^{50}Ar	13900	250	91(3)	8.7(3)
^{53}K$(p, 2p2n)$ ^{50}Ar	5837	245	86(6)	12.2(8)
^{51}Ar(p, pn) ^{50}Ar	1214	241	70(2)	45(2)

the time of flight was obtained from a scintillator placed in front of the target and a hodoscope located downstream of SAMURAI, which also provided an energy loss measurement from which the atomic number was inferred [31].

The high-efficiency γ-ray detector array DALI2$^+$ [34,35], composed of 226 NaI(Tl) detectors, was placed around MINOS to detect deexcitation γ rays. The array, which covered detection angles between $\approx$12° and $\approx$118° with respect to the center of the target, was calibrated in energy using standard ^{60}Co, ^{88}Y, ^{133}Ba, and ^{137}Cs sources. The full-energy-peak efficiency of the array, determined using a detailed GEANT4 [36] simulation, was 30% at 1 MeV with an energy resolution of 11% for a source moving at a velocity of 0.6c. Previous results and further details from the same experiment can be found in Refs. [12,19,37,38].

III. RESULTS

Low-lying states in ^{50}Ar were populated by direct and indirect reactions. For each reaction channel inclusive cross sections were obtained using the effective transmission of ^{50}Ar (which includes the efficiency of the beam line detectors and the beam losses in the detectors and the target), measured to be 56.7(15)%, and the efficiency of MINOS for each reaction. Table I summarizes the number of events in each reaction channel, the mean incident beam energy, the experimental efficiency of MINOS, and the corresponding inclusive cross sections.

Doppler corrected γ-ray spectra were obtained using the reaction vertex and the velocity of the fragment reconstructed with MINOS. Peak-to-total ratio and detection efficiency were improved by adding up the energies of γ rays deposited in detectors up to 10 cm apart. To reduce the contribution of the low-energy atomic background, γ rays with energies below 100 keV in the laboratory frame of reference were not considered for the add-back.

Figure 1(a) shows the Doppler-corrected spectrum obtained following multinucleon removal reactions, when the γ-ray multiplicity (M_γ) was limited to a maximum of 4. The spectrum was fitted with simulated response functions of the DALI2$^+$array and a double exponential function used to model the low- and high-energy background. The slopes of the
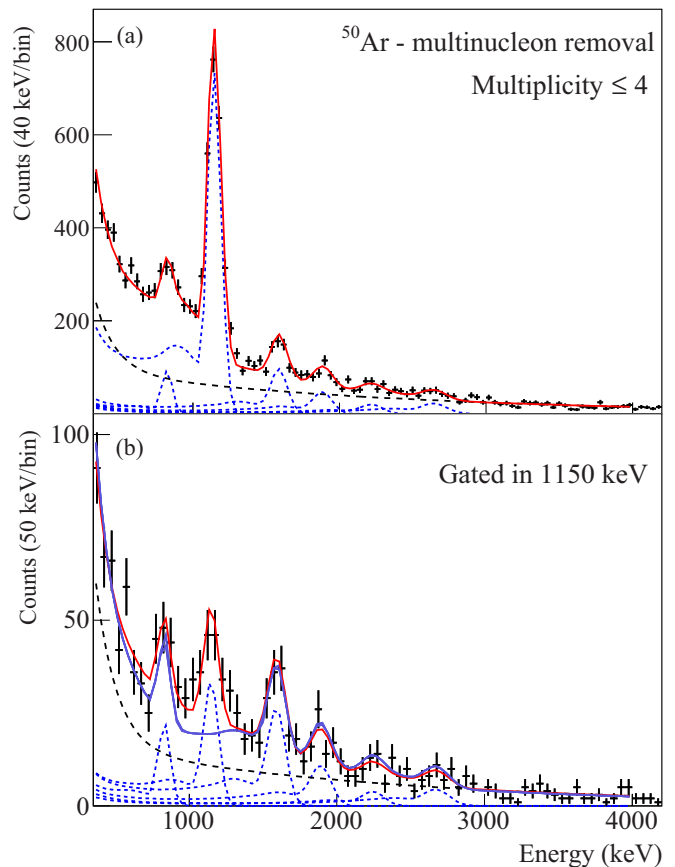

FIG. 1. (a) Doppler-corrected γ-ray spectrum obtained for ^{50}Ar populated from multinucleon removal reactions. The dashed blue lines represent the simulated responses of DALI2$^+$ to the different transitions, the dashed black line shows the fitted double-exponential background, and the solid red line shows the total fit. (b) γ-ray spectrum gated at $\approx$1150 keV. The best fit is shown by the solid red line while the expected counts are shown by the darker line.

two exponential functions were fixed by independent fits of the high- and low-energy regions. Six transitions at 826(7)(8), 1151(1)(12), 1593(6)(16), 1892(11)(19), 2227(19)(22), and 2657(21)(27) keV provided the best fit to the spectrum. The first reported uncertainty corresponds to the statistical error from the fit, while the second is the systematic error arising from the calibration of the γ-ray detectors and the possible lifetime of the states. To place the observed transitions in a level scheme, $\gamma\gamma$ coincidences were investigated. Figure 1(b) displays the γ-ray spectrum gated between 1090 and 1210 keV. A single background gate between 3000 and 4000 keV was used. Due to the many transitions observed in the spectrum it was not possible to place a more appropriate background gate. As a results, the transition where the gate was placed could not be completely removed by the background subtraction. Hence, the possibility of a doublet cannot be fully excluded. The best fit to the resulting spectrum, shown by the red line, was obtained by using the same response functions as in Fig 1(a), suggesting that all the transitions are coincident with the one at $\approx$1150 keV. Calculations on the expected number of counts in the coincidence spectrum
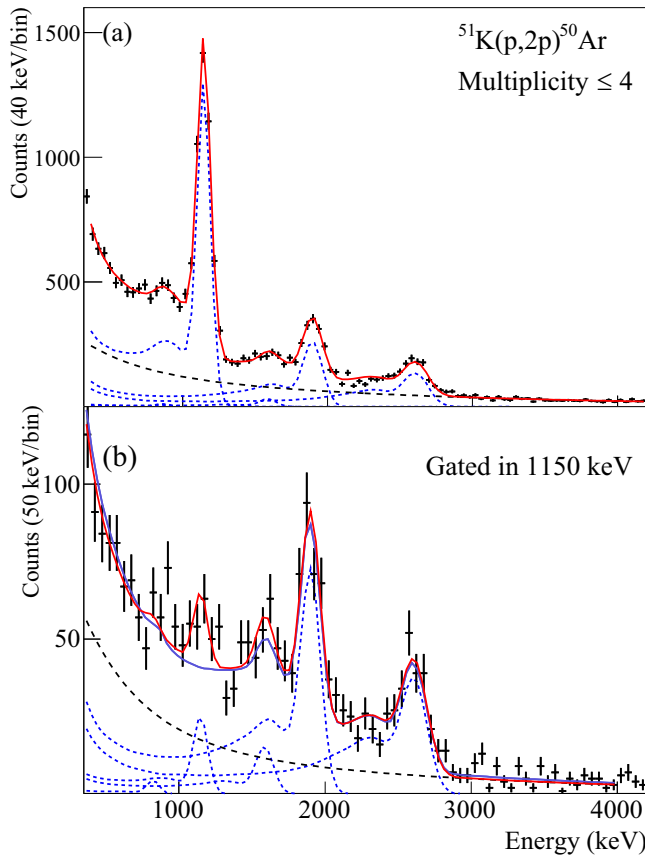
FIG. 2. Same as Fig. 1, but for the ^{51}K$(p, 2p)$^{50}Ar reaction.

FIG. 3. Same as Fig. 1, but for the ^{51}Ar(p, pn)^{50}Ar reaction.

obtained based on the area of the gate and the efficiency of DALI2$^+$are consistent with the observations, as shown by the blue line Fig. 1(b).

Figure 2(a) shows the Doppler-corrected spectrum obtained for ^{50}Ar produced by the proton-knockout reaction. A total of four peaks provided the best fit to the spectrum. The transition energies deduced from this spectrum are 1150(1)(11), 1592(23)(16), 1905(3)(19), and 2618(6)(26) keV. The spectrum resembles the one observed for the multinucleon removal, and in fact all of the transitions observed seem to correspond within uncertainties to transitions also present in Fig. 1. In this case, however, the intensity of the transition around ≈1600 keV is smaller, while the transitions at ≈1900 and ≈2600 keV are more intense. The transition observed in Fig. 1 at ≈824 was observed with a significance below 1σ, and the one at ≈2230 keV was not visible in this spectrum. The projection of the $\gamma\gamma$ matrix gated around ≈1150 keV is shown in Fig. 2(b). The best fit to the spectrum was obtained using the same four response functions used to fit the total spectrum, indicating that the transitions are coincident with the one at ≈1150 keV. As in the case of Fig. 1(a), it was not possible to completely remove the transition where the gate was placed by background subtraction. It is noted that, for the ^{51}K$(p, 2p)$^{50}Ar and the multinucleon removal reactions, gates around ≈1600, ≈1900, and ≈2600 keV only showed the reciprocal coincidence of these transitions with the one at ≈1150 keV.
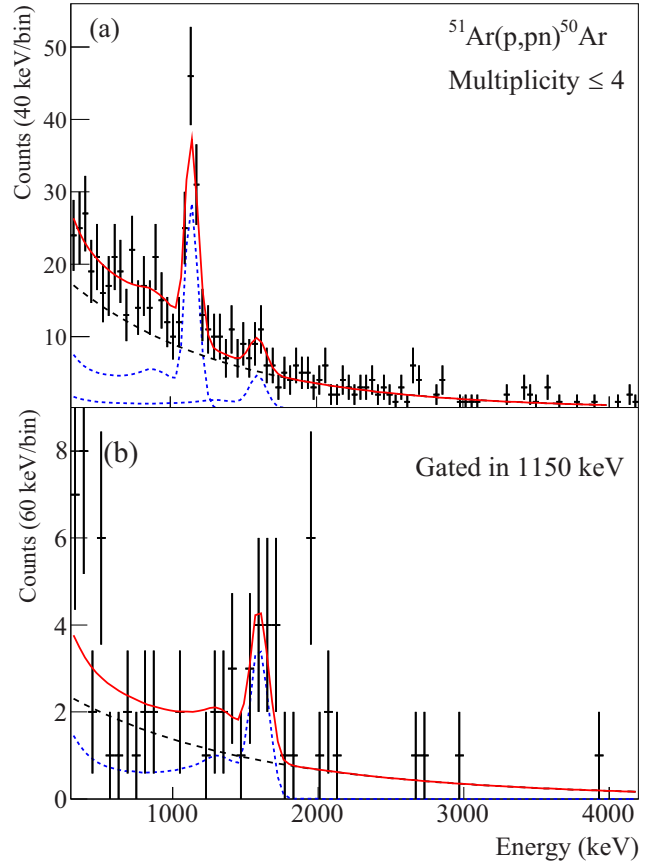
The Doppler-corrected spectrum corresponding to the ^{51}Ar(p, pn)^{50}Ar reaction is displayed in Fig. 3(a). Two peaks are visible in the spectrum with a significance above 2σ. The best fit yields transition energies of 1150(8)(11) and 1602(31)(16) keV. The $\gamma\gamma$ analysis shown in Fig. 3(b) clearly establishes the existence of the peak at ≈1600 keV, and shows that it is coincident with the one at ≈1150 keV. The energies observed in these spectrum are consistent with the ones obtained previously, suggesting the population of the same levels.

Figure 4(a) shows the Doppler-corrected spectrum obtained for the ^{50}Ar(p, p')^{50}Ar reaction. Three transitions are visible and the transition energies obtained for this case are 1138(8)(11), 1626(33)(16), and 2890(31)(29) keV. The background-subtracted coincidence spectrum, in Fig. 4(b), shows that the transition at 2890 keV is coincident with the one at 1138 keV. No coincidence between the transitions at 1626 and 1138 keV was observed, which can be attributed to the reduced statistics.

Based on the $\gamma\gamma$ analysis discussed above, the tentative level scheme shown in Fig. 5(a) was constructed. The energies of low-lying states in ^{50}Ar were calculated as the weighted average of the values obtained from the different reactions, when applicable. The weights were determined based only on the statistical uncertainty, and the systematic error was added in quadrature. Being the one with the highest intensity, the 1150(12) keV transition was placed decaying directly into the
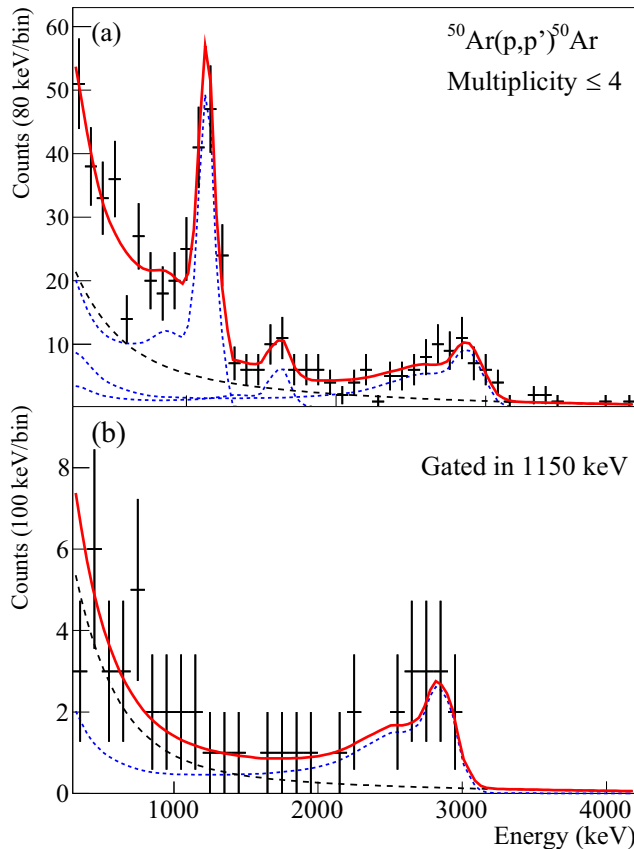
FIG. 4. Same as Fig. 1, but for the ^{50}Ar(p, p')^{50}Ar reaction.

ground state. This transition agrees, within error bars, with the one at 1178(18) keV reported in Ref. [20], where it was tentatively assigned to the $2_1^+ \rightarrow 0_{gs}^+$ transition. The transitions at 826(9), 1594(16), 1903(19), 2227(30), and 2621(32) keV were placed feeding the (2_1^+) state, in parallel to each other, depopulating states at 1976(15), 2744(20), 3053(23), 3377(32), and 3771(34) keV, respectively. The transition at 1594(16) keV agrees with the one at 1582(38) keV reported in Ref. [20], where a 4_1^+ assignment was suggested. The transition at 2890(42) keV observed in the ^{50}Ar(p, p')^{50}Ar reaction was placed on top of the 2_1^+ state, depopulating a level at 4040(44) keV. It has been shown by previous measurements on ^{46}Ar [40], ^{50}Ca [41], and ^{54}Ti [42], that proton inelastic scattering populates preferentially 2^+, 4^+, and 3^- states, therefore a 3^- spin and parity can be reasonably assigned to this level. The spin assignment for the 2744(20) keV level, also observed in this reaction, could then be either 2^+ or 4^+. Further discussion on the possible spin and parity assignments for the levels obtained in this work will be presented below.

For the direct reactions, exclusive cross sections to populate each observed state were obtained from the fitted γ-ray intensities. Table II summarizes the adopted level energies and exclusive cross sections obtained in this work. Based on simulated angular distributions of the γ rays, an additional uncertainty of 4% has been included to account for possible alignment of the states. The ground state cross section was calculated by subtracting the exclusive cross sections from the

inclusive one reported in Table I. The high background level, low statistics, and limited resolution of DALI2$^+$ could prevent the observation of low-intensity, high-energy transitions feeding directly the 0_{gs}^+ state, therefore the ground-state cross section is prone to be overestimated. In addition, it was not possible to disentangle between the direct ^{51}Ar(p, pn)^{50}Ar reaction and the scattering followed by neutron emission, ^{51}Ar(p, p')^{51}Ar $\rightarrow$ ^{50}Ar $+n$; therefore, all the cross sections for this channel are to be considered as an upper limit.

IV. DISCUSSION

Predictions for the energies of low-lying states in ^{50}Ar were obtained within the shell-model framework using the SDPF-MU effective interaction [43] and considering the full sd and pf model space for protons and neutrons. The original Hamiltonian was modified [23] using experimental data on exotic Ca [10] and K [44] isotopes. These calculations have previously provided good agreement with the experimental $E(2_1^+)$ and $E(4_1^+)$ energies in neutron-rich Ar isotopes [20] and suggest an $N = 32$ gap of $\approx$3 MeV for ^{50}Ar. Although this gap is predicted to be of similar magnitude as for ^{52}Ca, the wave function of the 2_1^+ state for ^{50}Ar turns out to be more mixed than the one for ^{52}Ca, making the effect of this shell closure less evident [20].

Calculations were also performed using the *ab initio* VS-IMSRG approach using the chiral NN+3N interaction labeled 1.8/2.0 (EM) in Refs. [45,46]. This NN+3N interaction is based on chiral effective field theory [47,48], a low-energy effective theory of quantum chromodynamics, with low-energy constants fitted to the properties of the lightest nuclei up to ^{4}He. The same chiral interaction has been successfully used to study $E(2_1^+)$ in the Ar isotopic chain [19], as well as excitation spectra from oxygen [49] to nickel [50] and tin [51] isotopes. For the model spaces, the sd space was considered for the protons and the pf for the neutrons, preventing the calculation of negative parity states. As in previous works [19,49–51] the IMSRG(2) approximation, where all induced operators are truncated at the two-body level, was employed. The VS-IMSRG was used to decouple a valence-space Hamiltonian, which captures 3N forces between valence nucleons via an ensemble normal ordering, for each nucleus of interest [52].

Spectroscopic factors, C^2S, were calculated within each model. For the case of the ^{51}K$(p, 2p)$^{50}Ar reaction, the $J^\pi = 3/2^+$ ground state for ^{51}K was employed [44,53] and knockout from the sd shell was considered, leading to the population of positive parity states exclusively. For the case of the ^{51}Ar(p, pn)^{50}Ar reaction the predicted ground-state spin of $1/2^-$ for ^{51}Ar was assumed. Figures 5(b) and 5(c) show the level scheme obtained from the calculations where only positive-parity states with calculated $C^2S \geqslant 0.1$ for the ^{51}K$(p, 2p)$^{50}Ar or ^{51}Ar(p, pn)^{50}Ar reactions are displayed. The predictions for the 3^- state based on the SDPF-MU Hamiltonian will be discussed afterwards.

The $E(2_1^+)$ of ^{50}Ar is accurately reproduced by both calculations, and a 0_2^+ is predicted to be the next excited state. The experimental level at 1976(15) keV has a good agreement with this state. It is noted that the SPDF-MU calculations predict the 0_2^+ state of ^{56}Cr to be 1982.1 keV, in fair agreement with
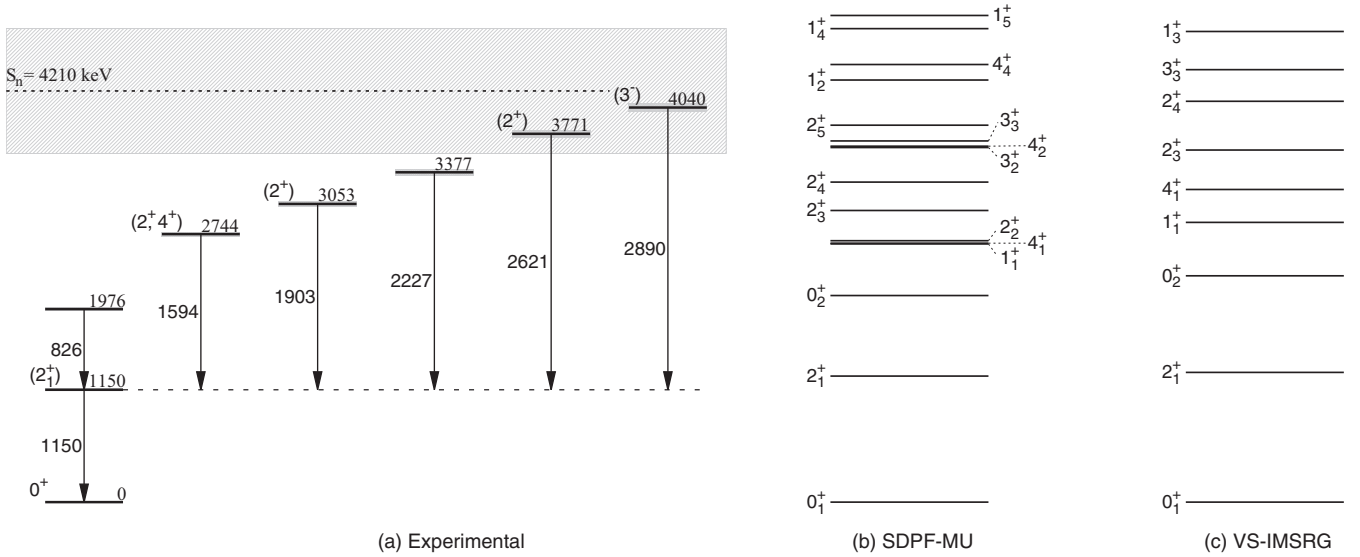
FIG. 5. (a) Experimental level scheme for ^{50}Ar deduced in the present work. Level and transition energies are given by the italic and regular fonts, respectively. The calculated neutron separation energy, S_n, is indicated [39]. Uncertainties in the energy levels are displayed as shaded areas. Parts (b) and (c) display predictions for low-lying states in ^{50}Ar by the SDPF-MU shell model and VS-IMSRG calculations, respectively.

the tentative experimental level at 1674.5(4) keV [54]. The structure at higher energies also presents many similarities: The next levels predicted to be populated are the 4_1^+, 1_1^+, 2_3^+ and 2_4^+. However, the energies predicted in the VS-IMSRG approach are modestly higher than in the SDPF-MU calculations. By enlarging the configuration space of this theoretical framework to include the sd-pf orbitals for protons and neutrons, additional excited states may appear at lower energies. The SDPF-MU calculations also predict significant population of more levels, in particular of the 2_2^+ and states with spin and parity 1^+ and 4^+.

To get an insight on the spin and parity of the observed levels, single-particle theoretical cross sections were computed in the distorted wave impulse approximation (DWIA) framework [55] using the Bohr-Mottelson single-particle potential [56]. For the optical potentials of the distorted waves, the microscopic folding model [57] with the Melbourne G-matrix interaction [58] and calculated nuclear density was

employed. The Franey-Love effective proton-proton interaction was adopted [59] and the spin-orbit part of each distorting potential was disregarded. Cross sections at different beam energies were calculated to take into account the energy loss of the beam in the thick target. The calculated single-particle cross sections were multiplied by the spectroscopic factors calculated for the reactions in each theoretical framework. Tables III and IV show the obtained results for the ^{51}K$(p, 2p)^{50}$Ar and ^{51}Ar$(p, pn)^{50}$Ar reactions, respectively.

The calculated ground state cross section for both reactions is much lower than the experimental values. As already mentioned, this is due to the nonobservation of states decaying directly to the 0_1^+ state, which results in an overestimation of the experimental cross section. For the case of the ^{51}K$(p, 2p)^{50}$Ar reaction, the SDPF-MU and VS-IMSRG calculations predict a cross section to the 2_1^+ state of 1.0 and 0.62 mb, respectively, in reasonable agreement with the experimental value of 0.8(2) mb. At higher energies the SPDF-MU calculation suggest the population of the 2_3^+, 2_4^+, and 2_5^+ states. Although high cross sections are also predicted for the 1_2^+ and 1_4^+ states, they would decay preferentially to the ground state, therefore its correspondence to any experimental level is unlikely. They may, however, account for the seeming too high experimental population of the ground state when compared to calculated cross sections. The VS-IMSRG calculation, on the other hand, only indicates the population of the 2_4^+ and 4_1^+ states. The fact that the VS-IMSRG calculations only predicts two states with sizable sd-proton cross sections is related with the reduced model space, which prevents proton pf-sd excitations. This in turn, highlights the importance of such excitations in the population of low-lying states. They have been investigated with a newly developed cross-shell VS-IMSRG approach [60]. In spite of the differences between the models, they both point out that the ^{51}K$(p, 2p)^{50}$Ar reaction mostly populates 2^+ states. The experimental levels

TABLE II. Energies of the low-lying states in ^{50}Ar measured in this work. The adopted levels were calculated as the weighted average of the results obtained for different reaction channels, when possible. Observed exclusive cross sections, σ_{exp}, for the direct reactions are reported.

Energy (keV)	$\sigma_{\text{exp}}^{(p,2p)}$ (mb)	$\sigma_{\text{exp}}^{(p,pn)}$ (mb)
0	$\leqslant 1.2(2)$	$\leqslant 26(4)$
1150(12)	0.8(2)	$\leqslant 15(4)$
1976(15)		
2744(20)	0.10(3)	$\leqslant 5(2)$
3053(23)	1.0(1)	
3377(32)		
3771(34)	0.8(1)	
4040(44)		

TABLE III. Calculated spectroscopic factors and cross sections for the states populated in the ^{51}K$(p, 2p)^{50}$Ar reaction.

| | | SPDF-MU | | | | VS-IMSRG | | | | |
| | | C^2S | | | σ_{theo} | | C^2S | | | σ_{theo} |
J^π	E (keV)	$1s_{1/2}$	$0d_{3/2}$	$0d_{5/2}$	(mb)	E (keV)	$1s_{1/2}$	$0d_{3/2}$	$0d_{5/2}$	(mb)
0_1^+	0		0.30		0.46	0		0.21		0.33
2_1^+	1291	0.23	0.38	0.01	1.00	1328	0.16	.21	0.02	0.62
4_1^+	2651			0.10	0.18	3201			0.15	0.25
2_3^+	2986	0.17	0.07		0.39					
2_4^+	3277	0.12	0.47	0.01	0.89	4104	0.16	0.79	0.02	1.43
2_5^+	3860	0.34	1.03		2.05					
1_2^+	4322	0.34			0.55					
1_4^+	4841	0.21	0.01		0.35					
				Total σ_{theo}	5.87				Total σ_{theo}	2.64

at 2744(20), 3053(23), and 3771(34) keV, observed in this reaction, are in fair agreement with the predictions for the 2_3^+, 2_4^+, and 2_5^+ states in the SDPF-MU model. We therefore tentatively assign this spin and parity to these states. The level at 2744(20) keV has been previously suggested to be the 4_1^+ [20]. Although the SDPF-MU calculations favors a 2^+ assignment, the comparison with the VS-IMSRG results make it also compatible with the 4_1^+. Furthermore, the population of this state in the ^{50}Ar$(p, p')^{50}$Ar reaction favors a 4_1^+ assignment. Therefore a $(2^+, 4^+)$ assignment is left open for this state. It is worth mentioning that the state at 1976(15) keV has a negligible cross section for the ^{51}K$(p, 2p)^{50}$Ar reaction, which is consistent with the theoretical predictions for the 0_2^+ state. The agreement between the SDPF-MU and VS-IMSRG calculations on the energy and spectroscopic factor of the 0_2^+ state suggest that it is spherical in nature, as the VS-IMSRG does not properly account for deformed low-lying states [37,50].

For the ^{51}Ar$(p, pn)^{50}$Ar reaction the theoretical models predict a 2_1^+ state cross section of $\approx$7–8 mb, while the experimental value is 15(4) mb. In this case, the experimental overestimation comes from the impossibility of distinguishing between the direct and indirect reactions in this channel. The next states with the higher predicted cross section are the 1_1^+, 4_1^+, and 2_3^+ states in both calculations. In the VS-IMSRG, population to the 3_3^+ state at 4428 keV is also predicted. As previously noted, the 1_1^+ state would most probably decay directly to the ground state. Furthermore, the 3_3^+ is not predicted by the VS-IMSRG to be populated in the ^{51}K$(p, 2p)^{50}$Ar reaction, so it is improbable that it corresponds to an experimental level. The ambiguity between the 2^+ and 4^+ characters for the state at 2744(20) keV observed in this reaction is therefore maintained.

Finally, theoretical predictions of the systematic of 3_1^- states for the $N = 32$ isotones have been obtained using the SDPF-MU calculations and confronted with available data

TABLE IV. Calculated spectroscopic factors and cross sections for the states populated in the ^{51}Ar$(p, pn)^{50}$Ar reaction.

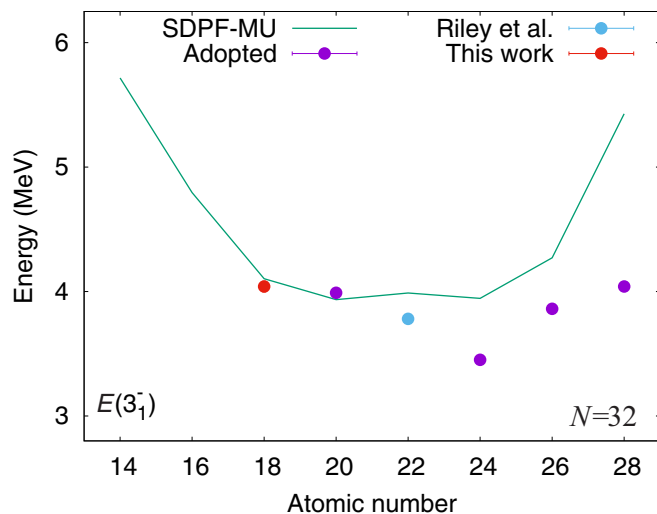| | | SPDF-MU | | | | | VS-IMSRG | | | | | |
| | | C^2S | | | | σ_{theo} | | C^2S | | | | σ_{theo} |
J^π	E (keV)	$0p_{1/2}$	$0p_{3/2}$	$0f_{5/2}$	$0f_{7/2}$	(mb)	E (keV)	$0p_{1/2}$	$0p_{3/2}$	$0f_{5/2}$	$0f_{7/2}$	(mb)
0_1^+	0	0.57				6.19	0	0.43				4.74
2_1^+	1291		0.73	0.05		7.29	1328		0.83			7.95
0_2^+	2115	0.28				2.28	2317	0.38				3.01
1_1^+	2643		0.91			7.05	2864		0.90			6.70
4_1^+	2651				0.93	5.33	3201				0.96	5.54
2_2^+	2676		0.25	0.05		2.34						
2_3^+	2986		0.73	0.02		5.47	3605		0.63			4.09
3_2^+	3631			0.05	0.40	2.34						
4_2^+	3644				0.11	0.56						
3_3^+	3698			0.03	0.70	3.79	4428				1.05	9.44
4_4^+	4481				0.23	1.26						
1_3^+							4819	0.15				0.67
1_5^+	4983	0.01	0.14			0.70						
					Total σ_{theo}	44.43					Total σ_{theo}	42.14

FIG. 6. Systematics of $E(3^-)$ for even-even $N = 32$ isotones. The circles represent the available data [42,61], including the value for ^{50}Ar reported in this work. The solid line shows the SDPF-MU calculations.

[42,61], including the state at 4040(44) keV obtained in this work, as shown in Fig. 6. The $E(3_1^-)$ for ^{50}Ar is comparable in magnitude to the one of ^{52}Ca, and the theoretical predictions show a good agreement with both isotopes, reinforcing the spin and parity assignments. However, the calculations overestimate the $E(3_1^-)$ as Z increases. For nuclei around Ca, the Fermi surface is located near the $Z = 20$ shell gap, therefore proton excitations require less energy. This is reflected in the calculations by the low 3^- levels predicted for ^{50}Ar, ^{52}Ca, and ^{54}Ti, where the calculations show a good agreement with the data. Going towards the Si isotopes, the excitation from the p shell to the sd shell becomes likely. This possible excitation is not taken into account in the calculations, which in turn increases the predicted $E(3_1^-)$ energies. On the other side, towards higher Z, the experimental levels are rather stable around 4 MeV, but the calculations are not able to reproduce them. In Ni, proton excitations from the sd to the pf shells as well as neutron excitations from the pf to the sdg shells may contribute. In particular, it has been reported that the neutron excitations from the pf to the sdg shells are not well reproduced due to a too large shell gap between pf and sdg shells, and it has been suggested that it is necessary to lower the sdg shell by 1 MeV to reproduce the negative parity states of Ni isotopes [62,63].

V. SUMMARY

Low-lying levels of ^{50}Ar have been investigated by proton- and neutron-knockout reactions, inelastic proton scattering, and multinucleon removal reactions. Based on the $\gamma\gamma$ analysis, a level scheme was constructed, including five newly observed transitions among which a candidate for the 3^- state has been reported for the first time. The experimental level scheme was compared to theoretical calculations performed in the SDPF-MU shell model, as well as the *ab initio* VS-IMSRG approach. Both calculations predict similar level schemes for ^{50}Ar. Theoretical cross sections for the ^{51}K$(p, 2p)$ ^{50}Ar and ^{51}Ar(p, pn) ^{50}Ar were compared to the observed ones, to infer the spin and parity of the states. Two of the newly observed states were tentatively assigned a (2^+) spin and parity, and it was shown that the state previously suggested to be the 4_1^+ could also correspond to a 2^+ state.

Overall, both theoretical calculations provide consistent results and a relatively good agreement with the experimental data for both the ^{51}K$(p, 2p)$ ^{50}Ar and ^{51}Ar(p, pn) ^{50}Ar reactions. This emphasizes the subshell closure at $N = 32$ and our understanding of shell evolution in this region. The remaining differences among calculations most likely arise from the reduced proton and neutron spaces employed in the VS-IMSRG and highlight their importance in understanding the low-lying structure of ^{50}Ar.

[1] O. Sorlin and M.-G. Porquet, Prog. Part. Nucl. Phys. **61**, 602 (2008).

[2] A. Ozawa, T. Kobayashi, T. Suzuki, K. Yoshida, and I. Tanihata, Phys. Rev. Lett. **84**, 5493 (2000).

[3] C. Hoffman *et al.*, Phys. Lett. B **672**, 17 (2009).

[4] R. Kanungo *et al.*, Phys. Rev. Lett. **102**, 152501 (2009).

[5] C. Détraz *et al.*, Phys. Rev. C **19**, 164 (1979).

[6] T. Motobayashi *et al.*, Phys. Lett. B **346**, 9 (1995).

[7] A. Huck *et al.*, Phys. Rev. C **31**, 2226 (1985).

[8] A. Gade *et al.*, Phys. Rev. C **74**, 021302 (2006).

[9] F. Wienholtz *et al.*, Nature (London) **498**, 346 (2013).

[10] D. Steppenbeck *et al.*, Nature (London) **502**, 207 (2013).

[11] S. Michimasa *et al.*, Phys. Rev. Lett. **121**, 022506 (2018).

[12] S. Chen *et al.*, Phys. Rev. Lett. **123**, 142501 (2019).

[13] R. Janssens *et al.*, Phys. Lett. B **546**, 55 (2002).

[14] J. Prisciandaro *et al.*, Phys. Lett. B **510**, 17 (2001).

[15] D.-C. Dinca *et al.*, Phys. Rev. C **71**, 041302 (2005).

[16] A. Buerger *et al.*, Phys. Lett. B **622**, 29 (2005).

[17] E. Leistenschneider *et al.*, Phys. Rev. Lett. **120**, 062503 (2018).

[18] S. N. Liddick *et al.*, Phys. Rev. Lett. **92**, 072502 (2004).

[19] H. N. Liu *et al.*, Phys. Rev. Lett. **122**, 072502 (2019).

[20] D. Steppenbeck *et al.*, Phys. Rev. Lett. **114**, 252501 (2015).

[21] T. Otsuka, T. Suzuki, R. Fujimoto, H. Grawe, and Y. Akaishi, Phys. Rev. Lett. **95**, 232502 (2005).

[22] T. Otsuka, T. Suzuki, M. Honma, Y. Utsuno, N. Tsunoda, K. Tsukiyama, and M. Hjorth-Jensen, Phys. Rev. Lett. **104**, 012501 (2010).

[23] Y. Utsuno *et al.*, JPS Conf. Proc. 6, 010007 (2015).

[24] T. Otsuka and T. Suzuki, Few-Body Syst. **54**, 891 (2013).

[25] J. D. Holt *et al.*, J. Phys. G **40**, 075105 (2013).

[26] J. D. Holt, J. Menendez, J. Simonis, and A. Schwenk, Phys. Rev. C **90**, 024312 (2014).

[27] K. Tsukiyama, S. K. Bogner, and A. Schwenk, Phys. Rev. C **85**, 061304 (2012).

[28] H. Hergert *et al.*, Phys. Rep. **621**, 165 (2016).

[29] S. R. Stroberg *et al.*, Annu. Rev. Nucl. Part. Sci. **69**, 307 (2019).

[30] T. Kubo *et al.*, Progr. Theor. Exp. Phys. **2012**, 03C003 (2012).

[31] T. Kobayashi *et al.*, Nucl. Instrum. Methods Phys. Res. B **317**, 294 (2013).

[32] A. Obertelli *et al.*, Eur. Phys. J. A **50**, 8 (2014).

[33] C. Santamaria *et al.*, Nucl. Instrum. Methods Phys. Res. A **905**, 138 (2018).

[34] S. Takeuchi *et al.*, Nucl. Instrum. Methods Phys. Res. A **763**, 596 (2014).

[35] I. Murray *et al.*, RIKEN Accel. Prog. Rep. **51**, 158 (2017).

[36] S. Agostinelli *et al.*, Nucl. Instrum. Methods Phys. Res. A **506**, 250 (2003).

[37] M. L. Cortés *et al.*, Phys. Lett. B **800**, 135071 (2020).

[38] Y. Sun *et al.*, Phys. Lett. B **802**, 135215 (2020).

[39] M. Wang *et al.*, Chin. Phys. C **41**, 030003 (2017).

[40] L. A. Riley *et al.*, Phys. Rev. C **72**, 024311 (2005).

[41] L. A. Riley *et al.*, Phys. Rev. C **90**, 011305 (2014).

[42] L. A. Riley *et al.*, Phys. Rev. C **96**, 064315 (2017).

[43] Y. Utsuno, T. Otsuka, B. A. Brown, M. Honma, T. Mizusaki, and N. Shimizu, Phys. Rev. C **86**, 051301 (2012).

[44] J. Papuga *et al.*, Phys. Rev. Lett. **110**, 172503 (2013).

[45] J. Simonis, S. R. Stroberg, K. Hebeler, J. D. Holt, and A. Schwenk, Phys. Rev. C **96**, 014303 (2017).

[46] K. Hebeler, S. K. Bogner, R. J. Furnstahl, A. Nogga, and A. Schwenk, Phys. Rev. C **83**, 031301 (2011).

[47] E. Epelbaum *et al.*, Rev. Mod. Phys. **81**, 1773 (2009).

[48] H.-W. Hammer *et al.*, Rev. Mod. Phys. **85**, 197 (2013).

[49] M. Ciemała *et al.*, Phys. Rev. C **101**, 021303 (2020).

[50] R. Taniuchi *et al.*, Nature (London) **569**, 53 (2019).

[51] T. D. Morris *et al.*, Phys. Rev. Lett. **120**, 152503 (2018).

[52] S. R. Stroberg, A. Calci, H. Hergert, J. D. Holt, S. K. Bogner, R. Roth, and A. Schwenk, Phys. Rev. Lett. **118**, 032502 (2017).

[53] J. Papuga *et al.*, Phys. Rev. C **90**, 034321 (2014).

[54] P. F. Mantica *et al.*, Phys. Rev. C **67**, 014311 (2003).

[55] T. Wakasa *et al.*, Prog. Part. Nucl. Phys. **96**, 32 (2017).

[56] A. Bohr and B. R. Mottelson, *Nuclear Structure*, 1st ed., Vol. 1 (W. A. Benjamin, New York, 1969).

[57] M. Toyokawa, K. Minomo, and M. Yahiro, Phys. Rev. C **88**, 054602 (2013).

[58] K. Amos *et al.*, in *Advances in Nuclear Physics*, edited by J. W. Negele and E. Vogt, Vol. 25 (Springer, US, 2000), Chap. 3, p. 275.

[59] M. A. Franey and W. G. Love, Phys. Rev. C **31**, 488 (1985).

[60] T. Miyagi *et al.*, Phys. Rev. C **102**, 034320 (2020).

[61] http://www.nndc.bnl.gov/ensdf/

[62] N. Shimizu *et al.*, Phys. Lett. B **753**, 13 (2016).

[63] Y. Utsuno *et al.*, Prog. Theor. Phys. Suppl. **196**, 304 (2012).